

1 Continuous Testing of Silica-PEI Adsorbents in a Lab.-Scale Twin 2 Bubbling Fluidized-Bed System

3

4 Jae-Young Kim^a, Je-Min Woo^a, Sung-Ho Jo^a, Seung-Yong Lee^a, Jong-Ho Moon^a, Hyunuk Kim^a,
5 Chang-Keun Yi^a, Hyojin Lee^a, Colin E. Snape^b, Lee Stevens^b, Chengong Sun^b, Hao Liu^b, [Jingjing](#)
6 [Liu](#)^b and Young Cheol Park^{a,†}

7

8 ^a*Korea Institute of Energy Research, 152 Gajeong-ro, Yuseong-gu, Daejeon 34129, Republic of*
9 *Korea*

10

11 ^b*University of Nottingham, Faculty of Engineering, The Energy Technologies Building, Triumph*
12 *Road, Nottingham, NG7 2TU, UK*

13

14 **Abstract**

15 In this study, a lab.-scale twin bubbling fluidized-bed system (TBS) has been used continuously
16 to test the performance for CO₂ adsorption of silica-PEI (S.PEI) adsorbents, containing 40 wt.%
17 of PEI, which were supplied by the University of Nottingham (UNOTT). The TBS comprises
18 bubbling-bed adsorption and desorption reactors, a riser for pneumatic conveying of solids from
19 the adsorption to the desorption reactor, and a cyclone for solid-gas separation. The adsorbent
20 prepared using PEI with a molecular mass of 800 (S.PEI-0.8K) was a preliminarily tested for
21 almost 24 hours at the given operating conditions by varying the [inlet sorbent/CO₂ mass ratio at](#)
22 [the adsorber](#) to analyse the CO₂ removal efficiency in the adsorption reactor and the dynamic
23 sorption capacity of the adsorbent. A 180-hour continuous test was then carried out by changing
24 various experimental conditions such as the H₂O concentration, reaction temperature, solid layer
25 height, reaction gas flow rate, and [inlet sorbent/CO₂ mass ratio at the adsorber](#) using PEI with a
26 molecular mass of 5000 (S.PEI-5K) adsorbent. [In this test, a CO₂ removal efficiency of above](#)
27 [80% and a dynamic sorption capacity greater than 6.0% were achieved.](#)

28

† To whom all correspondence should be addressed. E-mail: youngchp@kier.re.kr

29 Keywords: Post-combustion CO₂ capture; Dry solid sorbent; silica-PEI adsorbents; Lab.-scale
30 twin bubbling fluidized-bed system; Continuous performance test

31

32

33 **1. Introduction**

34 In an effort to address the global climate change issues, the international environmental
35 regulations on greenhouse gases have been strengthened, and the need for environmental
36 technology development has been emphasized. CO₂ emissions account for approximately 88% of
37 greenhouse gas emissions and a large part of CO₂ emissions come from fixed sources such as
38 power plants using fossil fuels (Joen and Sa, 2010; White et al., 2013). CO₂ concentration in the
39 atmosphere has exceeded 400 ppm and is estimated to increase to over 500 ppm by 2050 in case
40 without actions, which will increase the global average temperature (IPCC, 2013). Since the
41 operation of power plants using fossil fuels is expected to operate continuously in the future,
42 strategies to reduce the CO₂ concentration are necessary (D'Alessandro et al., 2010; Haszeldine,
43 2009). Recently, much attention has been given of late to the economical and environment-
44 friendly carbon capture, utilization and storage (CCUS) technology for collecting the emitted CO₂
45 from thermal power plants. The implementation of CCUS technology in power plants has been
46 proposed as a means to enable the continuous use of fossil fuels in the short term. In particular,
47 post-combustion CO₂ capture is drawing significant attention because it is easily applicable to
48 existing power plants (D'Alessandro et al., 2010; Haszeldine, 2009).

49 Among the various approaches to CO₂ capture, post-combustion CO₂ capture using amine
50 aqueous solution has been researched intensively and has been used in industries for over five
51 decades (D'Alessandro et al., 2010; Rochelle, 2009). However, the process using amine aqueous
52 solution has several limitations, including high energy demand for and environmental problems
53 such as volatile amine loss and reactor corrosion (Nguyen et al., 2010; Figueroa et al., 2008). To
54 overcome these limitations, non-corrosive dry solid particles with a low **regeneration** energy
55 penalty have been proposed as potential alternatives to liquid adsorbents (Choi et al., 2009; Bollini
56 et al., 2011; Wang et al., 2014). In particular, technology using dry solid particles is currently
57 being researched on as an innovative concept for CO₂ capture and recovery. Various solid
58 adsorbents have been researched, including adsorbents based on carbonates such as sodium,
59 potassium, and calcium (Liang et al., 2004; Lee et al., 2008; Fang et al., 2009; Lee et al., 2011),

60 zeolites (Shang et al., 2012), carbons (Hao et al., 2011), metal–organic frameworks (MOFs)
61 (Mason et al., 2011; Chaikittisilp et al., 2011), and amine-modified porous materials (Kim et al.,
62 2016; Choi et al., 2016; Min et al., 2017, 2018). In particular, amine-modified adsorbents have
63 been researched extensively because they can effectively CO₂ adsorption in exhaust gases
64 containing vapors.

65 However, few studies on the post-combustion CO₂ capture with amine-modified adsorbents at
66 pilot-scale process have been reported. ADA Environmental Solution (ADA-ES) has developed
67 a new concept reactor by incorporating staged fluidized beds for adsorption and a single fluidized
68 bed for regeneration to take advantage of the properties of functionalized amines sorbent. ADA-
69 ES has performed studies on CO₂ capture in a 1 MWe-scale process, and reported that the amine
70 adsorbent can achieve 90% CO₂ capture. (Krutka et al., 2013; Morris et al., 2014). Research
71 Triangle Institute (RTI) has developed an advanced solid sorbent-based CO₂ capture process for
72 application to exhaust gas from various industrial sources including coal-fired power plants,
73 NGCC power plants, and cement plants. RTI International has performed a bench-scale
74 demonstration tests and economic analyses related to diverse CO₂ emission sources using a
75 sorbent material that is based on a poly-amine (PEI) loaded on a silica initially developed at
76 Pennsylvania State University. (Nelson et al., 2017). The University of Nottingham (UNOTT)
77 has developed polyethyleneimine (PEI)-based sorbent for post-combustion CO₂ capture (Drage
78 et al., 2008, 2012). Zhang et al. evaluated using a laboratory-scale bubbling fluidized bed reactor
79 loaded with a few kg adsorbent, the adsorption performance of PEI–silica adsorbent under
80 different working conditions including with and without the presence of moisture, different gas–
81 solid contact times, initial bed temperatures, and CO₂ partial pressures (Zhang et al., 2014). In
82 addition, Zhang et al. evaluated the most important parameters affecting the regeneration heat,
83 including the physical properties of the adsorbents and process related variables including the
84 heat of adsorption, specific heat capacity, working capacity, moisture adsorption of the PEI-silica
85 adsorbent, the swing temperature difference and the degree of heat recovery. They also estimated
86 the working capacity of the PEI-silica adsorbent using pseudo-equilibrium capacities obtained
87 from the isobaric TGA tests (Zhang et al., 2016). KIER has developed dry CO₂ capture technology
88 using solid sorbents, and related research is being conducted. The research results on CO₂ capture
89 in a laboratory-scale device have been steadily reported, and a pilot-scale CO₂ capture process
90 using dry adsorbents has been developed, consisting of a fluidized-bed-type adsorption reactor
91 and a regeneration reactor (Yi et al., 2007, 2008; Yi, 2009, 2010; Park et al., 2009a,b, 2011; Kim

92 et al., 2010, 2011). At present, the authors are continuing their research using dry adsorbents, and
93 are developing more economical and energy-efficient dry adsorbents and the CO₂ capture process
94 for commercial scale of 10 MWe (Park et al., 2013, 2014a,b, 2016; Kim et al., 2017).

95 In this study, experiments were conducted to evaluate the CO₂ capture performance of silica-
96 PEI adsorbent in a laboratory-scale twin bubbling fluidized-bed system (TBS). A 24-hour
97 preliminary test and 180-hour continuous operation were performed using two types of adsorbents
98 with different PEI molecular masses, and the CO₂ capture performance of the adsorbent was
99 evaluated.

102 **2. Experimental**

104 **2.1 Physical properties of materials**

106 The silica-PEI sorbent used in this study was prepared by UNOTT by impregnating a mass
107 fraction of 40 wt.% PEI into a commercial mesoporous silica support. In the experiments, two
108 types of silica-PEI adsorbents with different PEI molecular masses were used. Table 1
109 summarizes the PEI molecular mass, bulk density, average particle size, particle size distribution
110 and the attrition index.

112 (Table 1)

115 The bulk density of the silica-PEI adsorbent was measured using a measuring cylinder, and
116 the average value of five measurements was used. The attrition of the solid particles was measured
117 with a fluidized bed particle attrition test system according to the method of American Society for
118 Testing and Material (ASTM) D5757-95. The particle attrition was indicated using an attrition
119 index (AI), which was calculated based on the solid loss rate by attrition after 5 hours (AI(5)).
120 The average particle size and particle size distribution (PSD) of silica-PEI adsorbents were
121 verified using a particle size analyzer (S3500, Microtrac) and the average value of three
122 measurements was used.

125 **2.2 Apparatus**

127 A schematic diagram of the TBS used in this study is shown in Fig. 1. The rig consists of
128 bubbling fluidized-bed type adsorption and desorption reactors, a transport tube for recycling the
129 solid particles after adsorption, a cyclone for separating the gas and solid, a rotary valve for
130 adjusting the solid circulation amount, and an infrared (IR) gas analyzer (ABB, Advance Optima)
131 for measuring the gas concentrations before and after the reaction.

132 The adsorption and desorption reactors were fabricated as bubbling fluidized-beds with a 0.1
133 m inner diameter and a 1.0 m height. An air box with a perforated-plate-type gas distributor was
134 installed at the bottom of the reactor, and, for circulating the solid particles, an overflow type was
135 fabricated. A heater was installed outside the air box of each reactor to prevent partial cooling
136 inside the reactor (the gas inlet part), thus minimizing the temperature difference between the
137 injected gas and the inside of the reactor. A temperature control device was installed outside each
138 reactor, and a jacket-type heat exchanger was installed outside the adsorption reactor. A cooling
139 water with an adjusted temperature in the cooling water supplier ([auto chiller, HYUNDAI](#)
140 [ENGCO., LTD., Korea](#)) was supplied to the heat exchanger to adjust the temperature of the reactor
141 and to control the heat generated from the adsorption reaction. A heater was installed outside the
142 desorption reactor to heat the reactor and control the reaction temperature. The simulated gas was
143 used for the gas supplied to each reactor, and a device for injecting H₂O was installed in front of
144 each reactor. For the reaction gas of the adsorption reactor, the simulated gas with a mixture of
145 N₂ (99.99%), CO₂ (99.9% or higher), and H₂O was used. A bubbler was installed before the
146 adsorption reactor to generate vapor, which is required for simulating coal-fired flue gas
147 condition. A line heater was installed in the gas inlet pipe at the back of the bubbler to prevent
148 water condensation in the inlet gas. For the fluidizing gas supplied to the desorption reactor, the
149 simulated gas with a mixture of N₂ (99.99%) and H₂O was used. A water pump was installed
150 before the desorption reactor to inject moisture and adjust the amount of moisture flowing into
151 the reactor. In addition, a pre-heater was installed to heat the gas and vaporize the inflow liquid-
152 state H₂O. A heater was installed outside the desorption reactor to heat the reactor and control the
153 reaction temperature.

154 The transport tube for the solid particles was fabricated as a fast fluidized bed with a 0.02 m
155 inner diameter and a 4.0 m height. For the gas supplied to the transport tube, N₂ (99.99%) was
156 used. A pre-heater was installed before the transfer device to increase the temperature of the gas
157 and to prevent the cooling of the solid particles coming from the adsorption reactor. The gas
158 flowing into the transport tube transfers the solid particles to the main cyclone, which separates
159 gas and solid and supplies solid particles to the desorption reactor. For the gas injected into each
160 reactor, the concentration of the reaction gas (CO₂) and the inflow rate of the reactor were adjusted

161 using a mass flow controller (E5850, Brooks Instruments). Rotary valves were installed at the
162 bottom of the adsorption reactor, desorption reactor, and main cyclone. The circulation rate of the
163 solid particles was adjusted using the rotary valve. Resistor temperature detectors (RTDs) were
164 installed in each reactor, gas pipe, etc. The temperature of each point was measured, and the
165 temperatures of the reactor (or adsorbent) and gas were detected using the RTD. Furthermore, the
166 adsorbent and gas flow conditions were examined by installing a pressure gauge and a differential
167 pressure gauge. The humidity of the gas was measured using a thermo-hygrometer (C-310
168 multifunction sensor, KIMO INSTRUMENTS, France) at the reactor inlet and outlet, and the
169 humidity values measured before and after the reaction were compared. Furthermore, an IR gas
170 analyzer was installed to measure the gas (CO₂) before and after the reaction. The measurements
171 values obtained from the instruments (thermometer, differential pressure gauge, analyzer, etc.)
172 installed in the TBS were collected through a Programmable Logic Controller (PLC) and were
173 stored in the computer.

174

175

176

(Fig. 1)

177

178

179 **2.3 Experimental conditions and method**

180

181 A preliminary test in the TBS was performed using the S.PEI-0.8K adsorbent, and a 180-
182 hour continuous test was then performed using S.PEI-5K adsorbent. The flow rate of the gas
183 flowing into the adsorption and desorption reactors was set to 4.5 cm/s. Solid particles initially
184 charged into two reactors and they flow into the adsorption reactor from the desorption reactor
185 when solid circulation started. The solid particles flowing into the adsorption reactor flow into the
186 transport tube after the adsorption reaction. Those scattered in the transport pipe are captured in
187 the main cyclone and are recirculated to the desorption reactor. The solid circulation rate is
188 determined by the rotation speed of the rotary valve installed between the desorption reactor and
189 the adsorption reactor. *After setting the rotation speed of the rotary valve installed between the
190 desorption and reactors, when the other two rotary valves were stopped, the solid circulation rate
191 was calculated using the differential pressure value for the adsorption reactor which changes with
192 time and the bulk density of adsorbents.* During the solid circulation, the desorption reactor was
193 heated to the desorption reaction temperature (128-130°C). Before the continuous tests, the solid
194 particles were dried and regenerated for approximately 12 hours at the temperature of 130°C and
195 at a solid circulation rate of 4.20 kg/h. The continuous test was then started. During this test, the

196 gases at the inlet and outlet of the adsorption reactor and the outlet of desorption reactor were
197 measured by an IR gas analyzer. The amount of CO₂ adsorption and the CO₂ removal efficiency
198 were calculated using the CO₂ concentration measured by an IR gas analyzer at each point. The
199 dynamic sorption capacity was calculated based on the amount of CO₂ adsorption and the solid
200 circulation rates. The samples after the reaction were collected from the bottom of the reactor.
201 The samples collected after the reaction were compared with the samples before the reaction in
202 terms of average particle size and PSD.

203

204

205 *2.3.1 Preliminary test*

206

207 The experimental conditions used for the preliminary test using S.PEI-0.8K are summarized
208 in Table 2. For the inlet gas of the adsorption reactor, the simulated gas with a mixture of N₂ and
209 CO₂ was used. As a fluidizing gas, N₂ was injected into the desorption reactor. The experimental
210 conditions of the adsorption reactor were set as follows: inlet CO₂ concentration of 15 vol.%,
211 reaction temperature of 70°C, and differential pressure in the reactor of 300 mmH₂O. Those of
212 the desorption reactor were set as follows: reaction temperature of 130°C and differential pressure
213 in the reactor of 300 mmH₂O. And then, the CO₂ capture performance of the S.PEI-0.8K adsorbent
214 were examined according to the [inlet sorbent/CO₂ mass ratio at the adsorber](#).

215

216 (Table 2)

217

218 *2.3.2 180-hour continuous test*

219

220 The 180-hour continuous test was performed in the TBS to evaluate the CO₂ capture
221 performance of the S.PEI-5K adsorbent with the goal to achieve above 80% CO₂ removal
222 efficiency and above 6.0 wt.% dynamic sorption capacity. In order to determine the best operating
223 conditions, several variables such as the H₂O concentration at the inlet gas stream of both reactors,
224 reaction temperatures, solid height of the adsorption reactor, and the [inlet sorbent/CO₂ mass ratio
225 at the adsorber](#) have been considered. The experimental conditions used for the 180-hour
226 continuous test are summarized in Table 3.

227

228 (Table 3)

229

230 The simulated flue gas mixture of N₂, CO₂ and H₂O was used as the inlet gas for the adsorption

231 reactor and a mixture of N₂ and H₂O was used for the desorption reactor. The experimental
232 conditions of the adsorption reactor were set as follow: inlet CO₂ concentration of 14.6 vol.%,
233 inlet H₂O concentration of 3.3 vol.%, reaction temperature of 65°C, and differential pressure in
234 the reactor of 300 mmH₂O. Those of the desorption reactor were set as follows: inlet H₂O
235 concentration of 5.0 vol.%, reaction temperature of 130°C, and differential pressure in the reactor
236 of 300 mmH₂O. Furthermore, the solid circulation rate was set to 3.89 kg/hr. The operating
237 conditions were changed to achieve optimal performance. To examine H₂O adsorption and the
238 desorption behavior of the S.PEI-5K adsorbent, the H₂O injection to the desorption reactor was
239 stopped, and the concentration of the H₂O introduced to the adsorption reactor was increased.
240 When the H₂O injection was stopped, the effect of adsorption temperature on CO₂ capture
241 performance was investigated by decreasing the temperature to 65, 60, and 55°C. The effect of
242 the solid height of the adsorption reactor on CO₂ capture performance at the adsorption reactor
243 temperature of 55°C was also investigated. The differential pressure of the adsorption reactor,
244 which directly related with the solid bed height, was decreased to 300, 255, and 220 mmH₂O. The
245 differential pressure of the adsorption reactor was controlled by varying discharge rate of solid
246 particles. Because of the reactor shape, the minimum differential pressure of the reactor was 220
247 mmH₂O when solid circulation is possible. After the solid height variation test, the adsorption
248 and desorption reactors were operated with differential pressures of 300 and 250 mmH₂O,
249 respectively. After that, the temperature of the adsorption reactor was set to 65°C, and the effect
250 of the solid circulation rate on CO₂ capture performance was investigated. Finally the temperature
251 of the desorption reactor was decreased from 130 to 120°C after setting the solid circulation rate
252 of 3.89 kg/hr so the effect of desorption temperature on CO₂ capture performance could be
253 investigated.

254

255

256 **3. Results and Discussion**

257

258 **3.1 Preliminarily test**

259

260 Fig. 2 shows a preliminary test results using the S.PEI-0.8K adsorbent, presenting the CO₂
261 removal efficiency and the dynamic sorption capacity according to the [inlet sorbent/CO₂ mass](#)
262 [ratio at the adsorber](#). The calculation of the CO₂ removal efficiency and the dynamic sorption
263 capacity is as follows:

264

265 The CO₂ removal efficiency (%)

$$266 \quad = 1 - \frac{\text{outlet CO}_2 \text{ mole flow rate at the adsorption reactor (kmol/hr)}}{\text{inlet CO}_2 \text{ mole flow rate at the adsorption reactor (kmol/hr)}} \times 100 \quad (1)$$

267 The dynamic sorption capacity (wt. %)

$$268 \quad = \frac{\text{captured CO}_2 \text{ mass flow rate at the adsorption reactor (kg/hr)}}{\text{solid circulation rate (kg/hr)}} \times 100 \quad (2)$$

269

270 The inlet sorbent/CO₂ mass ratio at the adsorber is an important factor which affects the
271 adsorption capacity of solid particles. Thus, it is crucial to find the effect of inlet sorbent/CO₂
272 mass ratio at the adsorber and the effect of solid circulation rate on the CO₂ removal efficiency
273 and dynamic sorption capacity of the solid particles. The test results showed that the CO₂ removal
274 efficiency was 72.5, 84.2, 92.7, and 95.0% and the dynamic sorption capacity was 6.36, 5.05,
275 3.08, and 2.20 wt.% at inlet sorbent/CO₂ mass ratio at the adsorber of 7.3, 10.6, 19.2, and 27.4,
276 respectively. As the inlet sorbent/CO₂ mass ratio at the adsorber increased, the removal efficiency
277 also increased, but the dynamic sorption capacity decreased. Based on this test, it is possible to
278 achieve 80% of CO₂ removal efficiency and above 5.5 wt.% dynamic sorption capacity when the
279 inlet sorbent/CO₂ mass ratio at the adsorber is between 7.3 and 10.6.

280

281

282 (Fig. 2)

283

284 3.2 180-hour continuous test

285

286 Fig. 3 shows the results of the 180-hour continuous test using the S.PEI-5K adsorbent in the
287 TBS. Fig. 3(a) shows the CO₂ removal efficiency and inlet and outlet CO₂ concentration profiles
288 of the adsorption reactor. During the 180-hour continuous test, the CO₂ was introduced at the
289 specified concentration (14.6 or 15.2 vol.%) into the adsorption reactor. It can be seen that the
290 outlet CO₂ concentration after adsorption has changed depending on the operating condition.
291 From the beginning, 78~85% of CO₂ removal efficiency was maintained until 150 hours of
292 continuous operation. After 150 hours, the CO₂ removal efficiency changed greatly from 73% to
293 88% according to solid circulation rate and desorption temperature. Fig. 3(b) shows the dynamic
294 sorption capacity and solid circulation rate of the solid particles. Up to 150 hours of continuous
295 operation, the dynamic sorption capacity was maintained around 6.0~6.5 wt.%. Further, after 150
296 hours, the dynamic sorption capacity changed greatly from a minimum of 5.54 wt.% to a
297 maximum of 7.43 wt.% according to the changes in the solid circulation rate and desorption
298 temperature. Fig. 3(c) shows the inlet and outlet H₂O concentration profiles of the adsorption and

299 desorption reactors. The H₂O adsorption and desorption behavior of the solid particles were
300 investigated during the continuous operation. H₂O was introduced to the adsorption reactor at a
301 3.3 vol.% concentration, but after 60 hours of continuous operation, the H₂O concentration
302 increased above 6.5 vol.%. However, the outlet H₂O concentration increased slightly because the
303 amount of H₂O adsorbed by the solid particles increased as the inlet H₂O concentration to the
304 adsorption reactor increased. The outlet H₂O concentration was higher than inlet H₂O
305 concentration in the desorption reactor. Fig. 3(d) shows the temperature profiles of the adsorption
306 and desorption reactors. During the 180-hour continuous operation, the temperatures of the
307 adsorption and desorption reactors were maintained at the specified values. Fig. 3(e) shows the
308 differential pressure profiles of the adsorption and desorption reactors. The differential pressures
309 of the adsorption and desorption reactors were maintained at the specified values during the
310 continuous operation.

311

312

313

(Fig. 3)

314

315 Up to 90 hours, the performance of the adsorbent did not change much even when the
316 temperature of the adsorption reactor changed. Below 60°C, the CO₂ removal efficiency and the
317 dynamic sorption capacity were maintained at 84.2% and 6.4 wt.%, respectively. The sorption
318 capacity of the adsorbent was maintained very well at below 60°C, being consistent with coal-
319 fired flue gas temperature (55-60°C) after flue gas desulfurization (FGD).

320 After 120 hours, the differential pressure of the adsorption reactor decreased to 300, 255, and
321 220 mmH₂O. The CO₂ removal efficiency and the dynamic sorption capacity of the adsorbent did
322 not change much. The differential pressure of the reactor indicates the solid height, which is
323 related to the gas-solid contact time of the adsorbent. As the differential pressure of the reactor
324 increases, the solid bed height also increases, as well as, the gas-solid contact time of the adsorbent
325 increases. The increase in the differential pressure of the reactor can improve the CO₂ capture
326 performance of the adsorbent due to the increase in the gas-solid contact time. Zhang et al.
327 reported that an increase in gas-solid contact time can effectively increase the working capacity
328 as well as increase the inventory bed mass in the reactor (Zhang et al., 2014). However, it seems
329 that the solid height of the adsorption reactor had little effect on the CO₂ capture performance of
330 the adsorbent in the 180-hour continuous test. The minimum differential pressure at which solid
331 circulation is possible in the TBS is 220 mmH₂O. In the 180-hour continuous test, the gas-solid
332 contact time is 7.5 seconds in case of differential pressure in adsorption reactor of 220 mmH₂O.

333 In this continuous test, the CO₂ capture performance of the adsorbent did not changed

334 significantly until the gas-solid contact time decreased to 7.5 seconds. In addition, it was
335 confirmed that the CO₂ removal efficiency and the dynamic sorption capacity were maintained at
336 both above 80% and 6.0 wt.%, respectively. Based on the test, this means that the adsorbent have
337 a sufficient gas-solid contact time even at the minimum differential pressure condition in the TBS.

338 After 150 hours, the effect of the inlet sorbent/CO₂ mass ratio at the adsorber on CO₂ removal
339 efficiency and the dynamic sorption capacity. Fig. 4 shows the results according to the inlet
340 sorbent/CO₂ mass ratio at the adsorber. When the inlet sorbent/CO₂ mass ratio at the adsorber
341 increased to 11.2, 12.2, 13.2, 14.2 and 15.2, the CO₂ removal efficiency increased to 83.2, 83.9,
342 84.2, 87.5 and 88.1%, but the dynamic sorption capacity decreased to 7.43, 6.88, 6.39, 6.20 and
343 5.81 wt.%, respectively. Below the inlet sorbent/CO₂ mass ratio at the adsorber of 14.2, it is
344 capable of achieving both above 80% CO₂ removal efficiency and 6.0 wt.% dynamic sorption
345 capacity. This demonstrates that the S.PEI-5K adsorbent has an excellent dynamic sorption
346 capacity. Zhang et al. estimated the working capacity of a 40% PEI/silica adsorbent as 1.35
347 mmol/g (5.94 wt.%) using pseudo-equilibrium capacities obtained from the isobaric TGA tests
348 (Zhang et al., 2016).

349
350

(Fig. 4)

351
352
353

354 Immediately before finishing the continuous test, the effect of the desorption temperature on
355 the CO₂ removal efficiency and the dynamic sorption capacity was investigated. As shown in
356 Table 4, the CO₂ removal efficiency and the dynamic sorption capacity at the 120°C desorption
357 temperature were lower than those at the 130°C desorption temperature. The CO₂ capture
358 performance falls due to extent of CO₂ desorption decreasing.

359
360

(Table 4)

361
362

363 **3.3 Particle size distribution (PSD) before and after reaction**

364

365 Fig. 5(a) shows the particle size distributions of the S.PEI-0.8K adsorbent before and after the
366 preliminary test, this adsorbent having multiple peaks of PSD. The particle size distributions of
367 S.PEI-0.8K adsorbent before and after the reaction were 28-592 μm and 34-498 μm respectively.

368 After the preliminary test, 510 μm or larger particles were abraded and did not appear in the particle
369 size distribution. Furthermore, the 320-500 μm particles decreased, the 175-300 μm particles
370 increased, the 120-170 μm particles decreased, and the 65-120 μm particles increased. The particles
371 smaller than 60 μm were [separated in the cyclone and discharged from](#) the TBS and decreased
372 greatly. Fig. 5(b) shows the PSD of the S.PEI-5K adsorbent before and after the 180-hour
373 continuous test. This adsorbent has a uniform PSD giving a single maximum in the PSD. Before
374 and after the continuous operation, the S.PEI-5K adsorbent displayed the same particle size
375 distribution of 80-498 μm . After the continuous operation, the 320-500 μm particles decreased
376 significantly while the 175-300 μm particles increased. and, the 170 μm or smaller particles also
377 decreased.

378 In this test, the change in the particle size distribution of the silica-PEI adsorbent is considered
379 to be due to the attrition of the solid particles. When solid particles flow through the adsorption
380 reactor to the solid transport tube, the flow rate of the gas increases greatly. Due to the increased
381 flow rate of gas, collision of the solid particles constituting the fluidized bed occurs frequently.
382 The 320-500 μm particles showed the largest change in PSD, suggesting that the attrition of the
383 particles in this size range is the largest. The attrition of particles generates fine particles, which
384 are separated in [the cyclone and discharged from](#) the system. This is a factor causing particle loss
385 in the process operation. The attrition loss of solid particles leads to an economic loss in the
386 process operation. Therefore, considering long-term process operation, the S.PEI-5K adsorbent,
387 which has a smaller distribution of 320-500 μm and smaller attrition index of 2.09, are considered
388 more advantageous for the fluidized bed process than S.PEI-0.8K adsorbent.

389
390

(Fig. 5)

391
392

393 **4. Conclusions**

394

395 1) The preliminary test using the S.PEI-0.8K adsorbent showed that when the [inlet sorbent/CO₂](#)
396 [mass ratio at the adsorber](#) increased to 7.3, 10.6, 19.2, and 27.4, the CO₂ removal efficiency
397 increased to 72.5, 84.2, 92.7, and 95.0%, while the dynamic sorption capacity decreased to
398 6.36, 5.05, 3.08, and 2.20 wt.%, respectively. It is possible to achieve 80% CO₂ removal

399 efficiency and 5.5 wt.% dynamic sorption capacity at the [inlet sorbent/CO₂ mass ratio at the](#)
400 [adsorber](#) between 7.3 and 10.6.

401 2) The 180-hour continuous test using the S.PEI-5K adsorbent showed the CO₂ capture
402 performance of adsorbent has been the CO₂ removal efficiency of 84.2% and the dynamic
403 sorption capacity of 6.4% when temperatures in adsorption reactor of below 60°C. It was
404 confirmed that the sorption capacity of the adsorbent was excellent at below 60°C adsorption
405 temperatures.

406 3) In the 180-hour continuous test, a CO₂ removal efficiency of above 80% and a dynamic sorption
407 capacity of above 6.0% were continuously maintained until the differential pressure of the
408 adsorption reactor decreased from 300 to 220 mmH₂O. This means that S.PEI-5K adsorbent
409 had a sufficiently long gas-solid contact time (7.5 sec) even at the minimum differential
410 pressure condition (220 mmH₂O) in the TBS.

411 4) In the 180-hour continuous test, the CO₂ removal efficiency increased but the dynamic sorption
412 capacity decreased when the [inlet sorbent/CO₂ mass ratio at the adsorber](#) increased. Below the
413 [inlet sorbent/CO₂ mass ratio at the adsorber](#) of 14.2, it is capable of achieving both above 80%
414 CO₂ removal efficiency and 6.0 wt.% dynamic sorption capacity.

415 5) In the 180-hour continuous test, the CO₂ removal efficiency and the dynamic sorption capacity
416 decreased when the desorption temperature was decreased from 130 to 120°C due to less CO₂
417 being desorbed.

418 6) The particle size analysis results, confirmed a change in the particle size distribution after the
419 test, due to attrition. In particular, the attrition of the 320-500µm particles was the largest. When
420 long-term process operation using the silica-PEI adsorbent is considered, S.PEI-5K adsorbents,
421 which have a smaller particle size distribution of 320-500 µm and smaller attrition index of 2.09,
422 appear to be appropriate for application to the fluidized bed process. These adsorbents can
423 provide economic benefit in process operation considering the life cycle and attrition loss of
424 solid particles.

425

426

427 **Acknowledgements**

428

429 This work was supported by the Korea Institute of Energy Technology Evaluation and
430 Planning (KETEP) and the Ministry of Trade, Industry & Energy (MOTIE) of the Republic of
431 Korea (No. 20158510011280)

432

433

434 **References**

435

436 Bollini, P., Didas, S. A., Jones, C. W., 2011. Amine-oxide hybrid materials for acid gas
437 separations. *Journal Materials Chemistry* 21, 15100-15120.

438 Chaikittisilp, W., Kim, H. J., Jones, C. W., 2011. Mesoporous alumina-supported amines as
439 potential steam-stable adsorbents for capturing CO₂ from simulated flue gas and ambient air.
440 *Energy & Fuels* 25, 5528-5537.

441 Choi, S., Drese, J. H., Jones, C. W., 2009. Adsorbent materials for carbon dioxide capture from
442 large anthropogenic point sources. *ChemSusChem* 2, 796-854.

443 Choi, W., Min, K., Kim, C., Ko, Y. S., Jeon, J. W., Seo, H., Park, Y.-K., Choi, M., 2016. Epoxide-
444 functionalization of polyethyleneimine for synthesis of stable carbon dioxide adsorbent in
445 temperature swing adsorption. *Nature Communications* 7, No. 12640.

446 D'Alessandro, D. M., Smit, B., Long, J. R., 2010. Carbon dioxide capture: prospects for new
447 materials. *Angewandte Chemie International Edition* 49 (35), 6058–6082.

448 Drage, T. C., A. Arenillas, A., Smith, K. M., Snape, C. E., 2008. Thermal stability of
449 polyethyleneimine based carbon dioxide adsorbents and its influence on selection of
450 regeneration strategies. *Microporous and Mesoporous Materials* 116, 504–512.

451 Drage, T. C., Snape, C. E., Stevens, L. A., Wood, J., Wang, J., Cooper, A. I., Dawson, R., Guo,
452 X., Satterley, C., Irons, R., 2012. Materials challenges for the development of solid sorbents
453 for post-combustion carbon capture. *Journal Materials Chemistry* 22, 2815.

454 Fang, F., Li, Z., Cai, N., 2009. Continuous CO₂ capture from flue gases using a dual fluidized bed
455 reactor with calcium-based sorbent. *Industrial & Engineering Chemistry Research* 48 (24),
456 11140-11147.

457 Figueroa, J. D., Fout, T., Plasynski, S., McIlvried, H., Srivastava, R. D., 2008. Advances in CO₂
458 capture technology—the U.S. department of energy's carbon sequestration program.
459 *International Journal of Greenhouse Gas Control* 2, 9-20.

460 Haszeldine, R. S., 2009. Carbon capture and storage: how green can black be?. *Science* 325,

461 1647–1652.

462 Hao, G.-P., Li, W.-C., Qian, D., Wang, G.-H., Zhang, W.-P., Zhang, T., Wang, A.-Q., Scheth, F.,
463 Bongard, H.-J., Lu, A.-H., 2011. Structurally designed synthesis of mechanically stable poly
464 (benzoxazine-co-resol)-based porous carbon monoliths and their application as high-
465 performance CO₂ capture sorbents. *Journal of American Chemical Society* 133, 11378–
466 11388.

467 International Panel on Climate Control (IPCC), 2013. Summary for Policymakers. In *Climate*
468 *Change 2013: The Physical Science Basis*; Cambridge University Press. Cambridge, MA.

469 Jeon, E. C., Sa, J. H., 2010. Development of CO₂ emission factor by fuel and CO₂ analysis at sub-
470 bituminous fired power plant. *Journal of Environment Health Science* 36(2), 128-135.

471 Kim, C., Cho, H. S., Chang, S., Cho, S. J., Choi, M., 2016. An ethylenediamine-grafted Y zeolite:
472 a highly regenerable carbon dioxide adsorbent via temperature swing adsorption without
473 urea formation. *Energy & Environmental Science* 9, 1803–1811.

474 Kim, J. -Y., Lim, H., Woo, J. M., Jo, S. -H., Moon, J. -H., Lee S. -Y., Lee H., Yi, C. -K. 2017.
475 Performance evaluation of K-based solid sorbents depending on the internal structure of the
476 carbonator in the bench-scale CO₂ capture process. *Korean Chemical Engineering Research*
477 55 (3), 419-425.

478 Kim, K. -C., Kim. K. Y., Park, Y. C., Jo, S. -H., Ryu, H. J., Yi, C. K., 2010. Study of
479 hydrodynamics and reaction characteristics of K-based solid sorbents for CO₂ capture in a
480 continuous system composed of two bubbling fluidized-bed reactors. *Korean Chemical*
481 *Engineering Research* 48 (4), 499-505.

482 Kim, K. -C., Park, Y. C., Jo, S. -H., Yi, C. K., 2011. The effect of CO₂ or steam partial pressure
483 in the regeneration of solid sorbents on the CO₂ capture efficiency in the two-interconnected
484 bubbling fluidized-beds system. *Korean Journal of Chemical Engineering* 28 (10), 1986-
485 1989.

486 Krutka, H., Sjostroma, S., Starnsa, T., Dillona, M., Silvermanb, R., 2013. Post-combustion CO₂
487 capture using solid sorbents: 1 MWe pilot evaluation. *Energy Procedia* 37, 73-88.

488 Lee, J. B., Ryu, C. K., Baek, J.-I., Lee, J. H., Eom, T. H., Kim, S. H., 2008. Sodium-based dry
489 regenerable sorbent for carbon dioxide capture from power plant flue gas. *Industrial and*
490 *Engineering Chemistry Research* 47 (13), 4465-4472.

491 Lee, S. C., Chae, H. J., Choi, B. Y., Jung, S. Y., Ryu, C. Y., Park, J. J., Baek, J. -I., Ryu, C. K.,
492 2011. The effect of relative humidity on CO₂ capture capacity of potassium-based sorbents.
493 *Korean Journal of Chemical Engineering* 28 (2), 480-486.

494 Liang, Y., Harrison, D. P., Gupta, R. P., Green, D. A., McMichael, W. J., 2004. Carbon dioxide

495 capture using dry sodium-based sorbents. *Energy & Fuels* 18 (2), 569-575.

496 Mason, J. A., Sumida, K., Herm, Z. R., Krishna, R., Long, J. R., 2011. Evaluating metal-organic
497 frameworks for post-combustion carbon dioxide capture via temperature swing adsorption.
498 *Energy & Environmental Science* 4, 3030-3040.

499 Min, K., Choi, W., Kim, C., Choi, M., 2018. Oxidation-stable amine-containing adsorbents for
500 carbon dioxide capture. *Nature Communications* 9, No. 726.

501 Min, K., Choi, W., Choi, M., 2017. Macroporous silica with thick framework for steam-stable
502 and high-performance poly(ethyleneimine)/silica CO₂ adsorbent. *ChemSusChem* 10, 2518-
503 2526.

504 Morris, W. J., Sjostrom, S., Sayyah, M., Denney, J., Syed, O., Lindsey, C., Lindsay, M., 2014.
505 ADA's solid sorbent CO₂ capture process: developing solid sorbent technology to provide
506 the necessary flexible CO₂ capture solutions for a wide range of applications. *Energy*
507 *Procedia* 63, 1536-1545.

508 Nelson, T. O., Kataria, A., Mobley, P., Soukri, M., Tanthana, J., 2017. RTI's solid sorbent-based
509 CO₂ capture process: technical and economic lessons learned for application in coal-fired,
510 NGCC, and cement plants. *Energy Procedia* 114, 1536-1545.

511 Nguyen, T., Hilliard, M., Rochelle, G. T., 2010. Amine volatility in CO₂ capture. *International*
512 *Journal of Greenhouse Gas Control* 4, 707-715.

513 Park, Y. C., Jo, S. -H., Bae, D. H., Min, B. M., Ryu, C. K., Yi, C. -K., 2014a. Development status
514 of the CO₂ capture process with dual fluidized-beds for post-combustion CCS technology in
515 Korea. *Proceedings of the 13th International Conference on Clean Energy* 1, 2730-2732.

516 Park, Y. C., Jo, S. -H., Kyung, D. -H., Kim, J. -Y., Yi, C. -K., Ryu, C. K., Shin, M. S., 2014b.
517 Test operation results of the 10 MWe-scale dry-sorbent CO₂ capture process integrated with
518 a real coal-fired power plant in Korea. *Energy Procedia* 63, 2261-2265.

519 Park, Y. C., Jo, S. -H., Lee, D. H., Yi, C. -K., Ryu, C. K., Kim, K. S., You, C. H., Park, K. S.,
520 2013. The status of the development project for the 10 MWe-scale dry-sorbent carbon
521 dioxide capture system to the real coal-fired power plant in Korea. *Energy Procedia* 37, 122-
522 6.

523 Park, Y. C., Jo, S. -H., Lee S. -Y., Moon, J. -H., C. -K., Ryu, Lee, J. B., Yi, C. -K., 2016.
524 Performance analysis of K-based KEP-CO₂P1 solid sorbents in a bench-scale continuous
525 dry-sorbent CO₂ capture process. *Korean Journal of Chemical Engineering* 33 (1), 73-79.

526 Park, Y. C., Jo, S. -H., Park, K. W., Park, Y. S., Yi, C. -K., 2009a. Effect of bed height on the
527 carbon dioxide capture by carbonation/regeneration cyclic operations using dry potassium-
528 based sorbents. *Korean Journal of Chemical Engineering*. 26, 874-878.

529 Park, Y. C., Jo, S. -H., Ryu, C. K., Yi, C. -K., 2009b. Long-term operation of carbon dioxide
530 capture system from a real coal-fired flue gas using dry regenerable potassium-based
531 sorbents. *Energy Procedia* 1, 1235-1239.

532 Park, Y. C., Jo, S. -H., Ryu, C. K., Yi, C. -K., 2011. Demonstration of pilot scale carbon dioxide
533 capture system using dry regenerable sorbents to the real coal-fired power plant in Korea.
534 *Energy Procedia* 4, 1508-1512.

535 Rochelle, G. T., 2009. Amine scrubbing for CO₂ capture. *Science* 325, 1652-1654.

536 Shang, J., Li, G., Singh, R., Gu, Q., Nairn, K. M., Bastow, T. J., Medhekar, N., Doherty, C. M.,
537 Hill, A. J., Liu, J. Z., Webley, P. A., 2012. Discriminative separation of gases by a ‘molecular
538 trapdoor’ mechanism in chabazite zeolites. *Journal of American Chemical Society* 134,
539 19246–19253.

540 Wang, J., Huang, L., Yang, R., Zhang, Z., Wu, J., Gao, Y., Wang, Q., O’Hare, D., Zhong, Z.,
541 2014. Recent advances in solid sorbents for CO₂ capture and new development trends.
542 *Energy & Environmental Science* 7, 3478-3518.

543 White, C. M., Strazisar, B. R., Granite, E. J., Hoffman, J. S., Pennline, H. W., 2013. Separation
544 and capture of CO₂ from large stationary sources and sequestration in geological formation-
545 coalbeds and deep saline aquifers. *Journal of the Air & Waste Management Association* 53,
546 645-715.

547 Yi, C. -K., 2009. Advances of carbon capture technology. *Korean Industrial Chemistry News*
548 12(1), 30-42.

549 Yi, C. -K., 2010. Advances of post-combustion carbon capture technology by dry sorbent. *Korean*
550 *Chemical Engineering Research* 48 (2), 140-146.

551 Yi, C. -K., Hong, S. W., Jo, S. -H., Son, J. E., Choi, J. H., 2005. Absorption and regeneration
552 characteristics of a sorbent for fluidized-bed CO₂ removal process. *Korean Chemical*
553 *Engineering Research* 43 (2), 294-298.

554 Yi, C. -K., Jo, S. -H., Seo, Y., 2008. The effect of voidage on the CO₂ sorption capacity of K-
555 based sorbent in a dual circulating fluidized bed process. *Journal of Chemical Engineering*
556 *of Japan* 41 (7), 691-694.

557 Yi, C. -K., Jo, S. -H., Seo, Y., Lee, J. B., Ryu, C. K., 2007. Continuous operation of the potassium-
558 based dry sorbent CO₂ capture process with two fluidized-bed reactors. *International Journal*
559 *of Greenhouse Gas Control*. 1 (1), 31-36.

560 Yi, C. -K., Jo, S. -H., Seo, Y., Moon, K. H., Yoo, J. S., 2006. CO₂ capture characteristics of dry
561 sorbents in a fast fluidized reactor. *Studies in Surface Science and Catalysis* 159, 501-504.

562 Zhang, W., Liu, H., Sun, C., Drage, T. C., Snape, C. E., 2014. Performance of polyethyleneimine–

563 silica adsorbent for post-combustion CO₂ capture in a bubbling fluidized bed. *Chemical*
564 *Engineering Journal* 251, 293–303.

565 [Zhang, W., Liu, H., Sun, Y., Cakstins, J., Sun, C., Snape, C. E., 2016. Parametric study on the](#)
566 [regeneration heat requirement of an amine-based solid adsorbent process for post-](#)
567 [combustion carbon capture. *Applied Energy* 168, 394-405.](#)

568

569

List of Tables

570

571

572 Table 1. Physical properties of silica-PEI (fresh sorbent).

573 Table 2. Summary of experimental conditions (Preliminarily test).

574 Table 3. Summary of experimental conditions (180-hour continuous test).

575 Table 4. The CO₂ removal efficiency and dynamic sorption capacity of S.PEI-5K adsorbent
576 according to different temperature of desorption reactor.

577

578

579

580

581 **Table 1**

582

	S.PEI-0.8K	S.PEI-5K
PEI molecular mass (g/mol)	800	5000
Bulk density (g/cm ³)	0.5608	0.5512
Average particle size (μm)	230	240
Particle distribution (μm)	28 ~ 592	80 ~ 498
Attrition index (%)	3.27	2.09

583

584

585 **Table 2**

586

Item	Adsorption reactor	Desorption reactor
Inlet flow rate (l/min)	17.0 ~ 20.0	14.8 ~ 15.1
Inlet H ₂ O concentration (vol.%)	-	-
Inlet CO ₂ concentration (vol.%)	14.3 ~ 14.6	-
Temperature (°C)	66 ~ 70	128 ~ 130
Differential pressure (mmH ₂ O)	280 ~ 300	280 ~ 300
Inlet sorbent/CO ₂ mass ratio at the adsorber (-)		7.3 ~ 27.4

587

588

589

590 **Table 3**

591

Item	Adsorption reactor	Desorption reactor
Inlet flow rate (l/min)	17.7 ~ 27.3	15.0 ~ 15.8
Inlet H ₂ O concentration (vol.%)	3.0 ~ 7.1	0 ~ 4.5
Inlet CO ₂ concentration (vol.%)	14.6 ~ 15.2	-
Temperature (°C)	56 ~ 66	119 ~ 130
Differential pressure (mmH ₂ O)	220 ~ 300	250 ~ 300
Inlet sorbent/CO ₂ mass ratio at the adsorber (-)	11.2 ~ 15.2	

592

593

594 **Table 4**

595

Item	Desorption reactor temperature (°C)	
	119 ~ 120	129 ~ 130
CO ₂ removal efficiency (%)	73.1	81.6
Dynamic sorption capacity (wt.%)	5.54	6.19

596

597

List of Figures

598

599

600 Figure 1. Schematic diagram of the TBS.

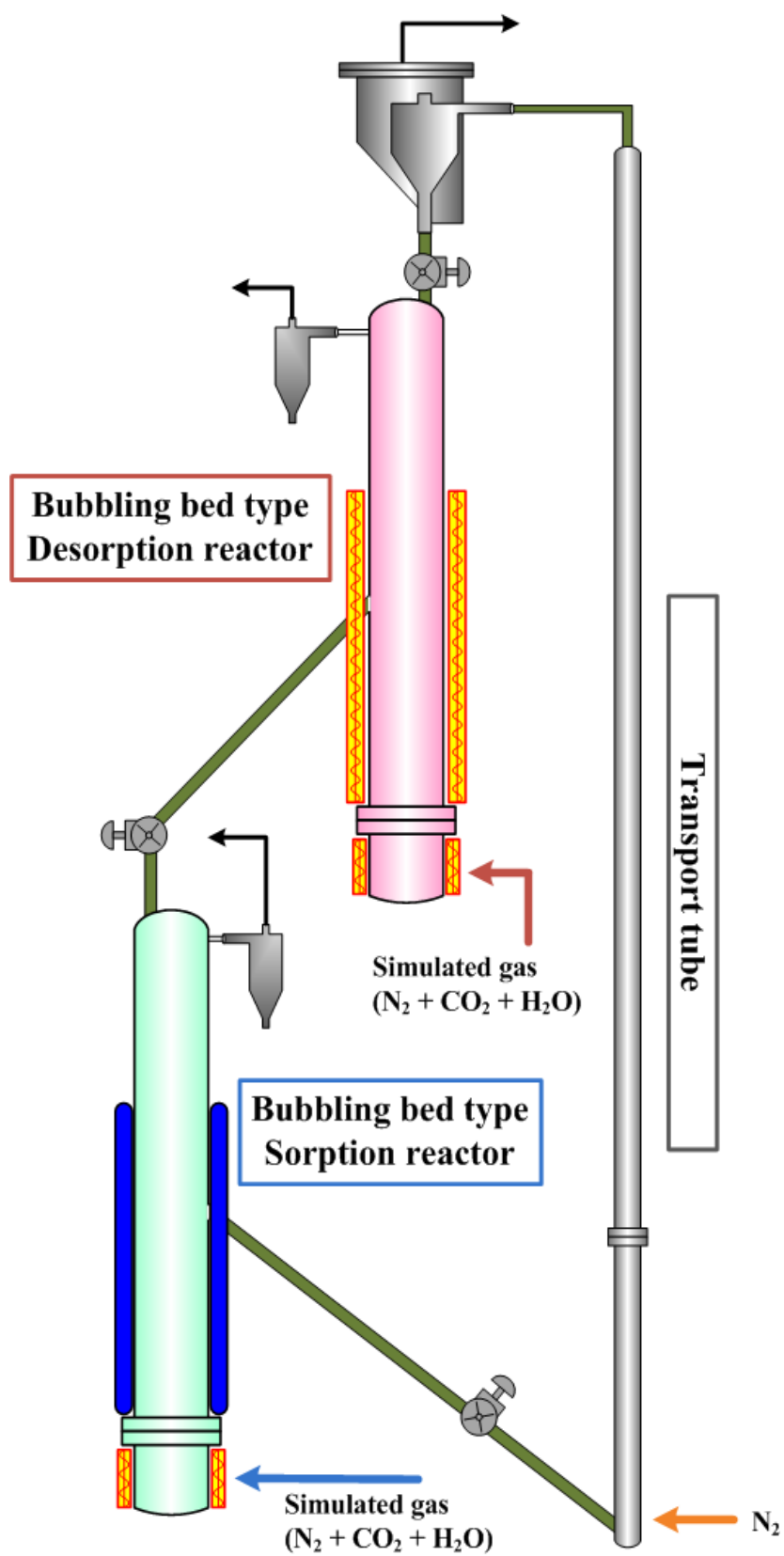
601 Figure 2. The CO₂ removal efficiency and dynamic sorption capacity of S.PEI-0.8K adsorbent
602 according to variation of inlet sorbent/CO₂ mass ratio at the adsorber (■ : CO₂ removal
603 efficiency, □ : dynamic sorption capacity).

604 Figure 3. Results for the 180-hour continuous test in the TBS, (a) CO₂ removal efficiency and
605 CO₂ concentration, (b) Dynamic sorption capacity and solid circulation rates, (c) H₂O
606 concentration, (d) Reactor temperature, (e) Differential pressure.

607 Figure 4. The CO₂ removal efficiency and dynamic sorption capacity of S.PEI-5K adsorbent
608 according to variation of inlet sorbent/CO₂ mass ratio at the adsorber (■ : CO₂ removal
609 efficiency, □ : dynamic sorption capacity).

610 Figure 5. Particle size distribution of silica-PEI sorbent (fresh and used), (a) Before and after the
611 preliminary test, (b) Before and after the 180-hour continuous test.

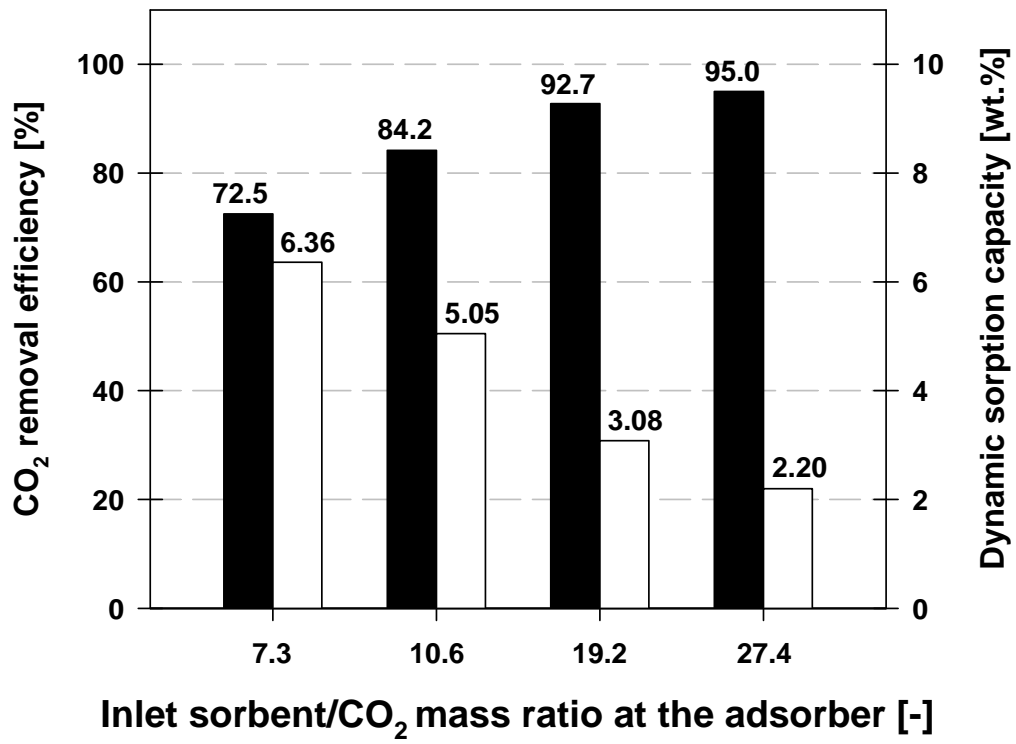
612



613

614 **Fig. 1.**

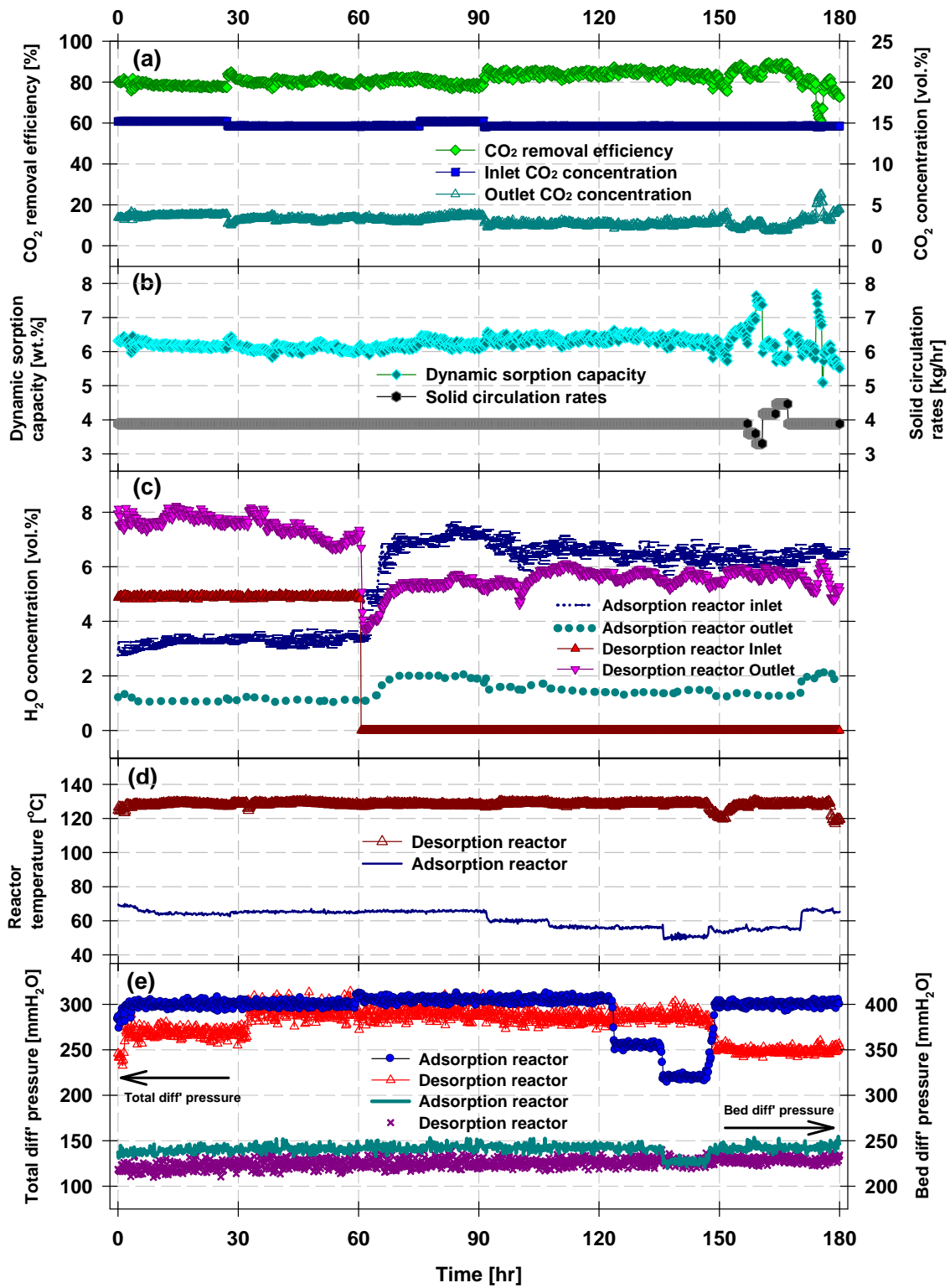
615



616

617 **Fig. 2.**

618

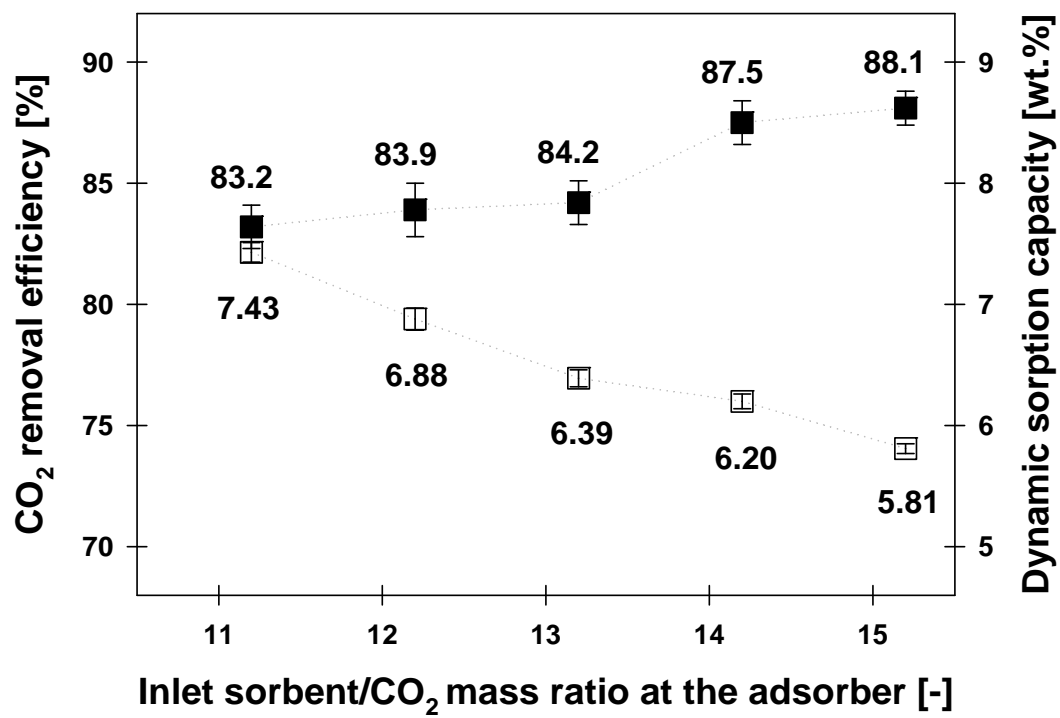


619

620

621 Fig. 3.

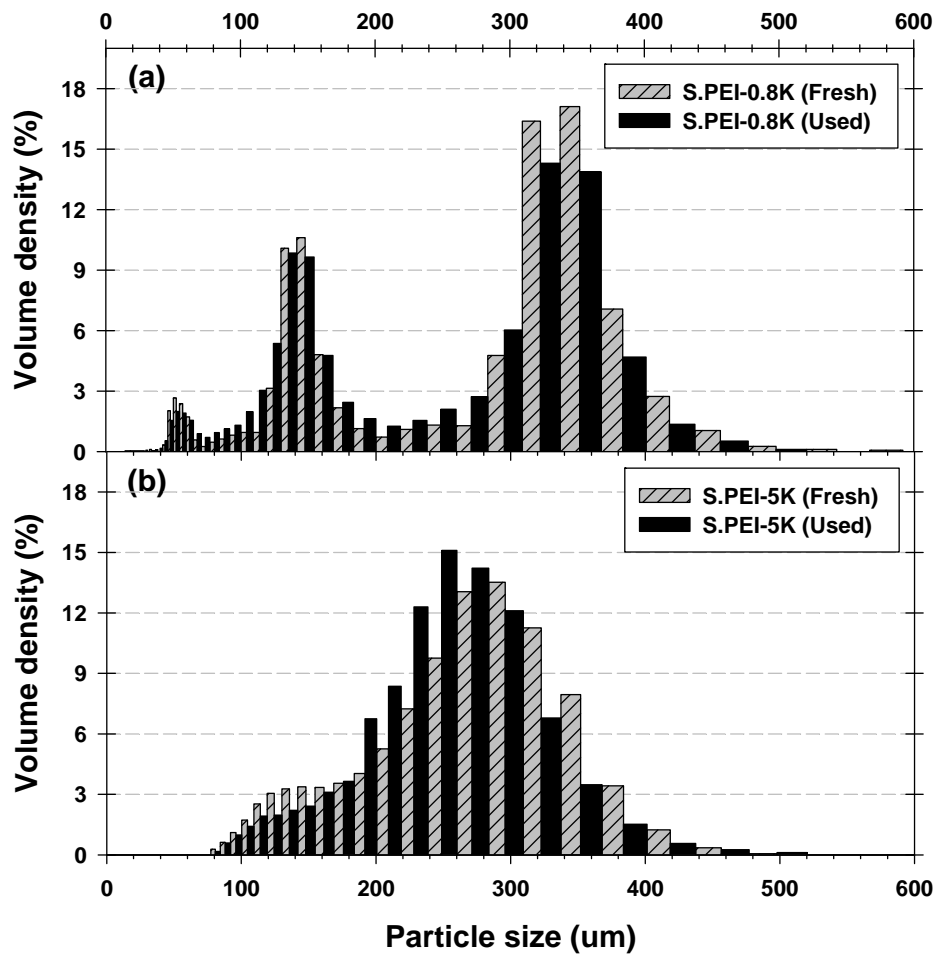
622



623

624 **Fig. 4.**

625



626

627 **Fig. 5.**

628